European Journal of Mechanics / B Fluids 72 (2018) 87–102

Contents lists available at ScienceDirect

European Journal of Mechanics / B Fluids

journal homepage: www.elsevier.com/locate/ejmflu

# Newtonian Poiseuille flow in ducts of annular-sector cross-sections with Navier slip

Sophia Kyritsi-Yiallourou [a], Georgios C. Georgiou [b,*]

[a] Section of Mathematics, Hellenic Naval Academy, Chatzikyriakou Avenue, 18539 Piraeus, Greece
[b] Department of Mathematics and Statistics, University of Cyprus, PO Box 20537, 1678 Nicosia, Cyprus

## HIGHLIGHTS

- The Newtonian Poiseuille flow in ducts of annular-sector or circular-sector cross-sections is considered.
- Navier slip is assumed to occur along the circular walls.
- A general analytical solution is derived for the above flow.
- The effects of the sector angle, the radii ratio and the slip number are analysed.

## ARTICLE INFO

*Article history:*
Received 5 April 2018
Received in revised form 1 May 2018
Accepted 2 May 2018

*Keywords:*
Poiseuille flow
Newtonian fluid
Navier slip
Circular sector
Annular sector

## ABSTRACT

We consider the Newtonian Poiseuille flow in a duct the cross section of which is either a circular or an annular sector assuming that Navier slip occurs either along both the cylindrical walls or only along the outer cylindrical wall. A general analytical solution is derived and the results for the latter case are discussed and the effects of the angle of the sector, the radii ratio and the slip number are analysed.



## 1. Introduction

The classical Poiseuille, i.e. pressure-driven, flow in ducts of various cross sections has regained interest in the past few decades, due to its application in micro- and nanofluidics [1,2]. Such applications include micro- and macro-fabrication technologies, micro-electro-mechanical systems (MEMS), computer chips, chemical separations, medical and biomedical procedures etc. Morini [3] pointed out that the cross-sectional shape of a microchannel strongly depends on the technology used to build it and that it is possible to have microchannels of any cross-section. For example, tubes of semi-circular cross section are used in hard micromachining with isotropic etching [2]. Annular-sector ducts are applicable to multi-passage internally finned tubes [4] or ducts which need to conform to a curved boundary [5].

Slip effects are also very important in microfluidic applications [1,6]. It is well established that even Newtonian liquids may exhibit slip [7]. Neto et al. [7] reviewed experimental studies of wall slip of Newtonian liquids and discussed the effects of surface roughness, wettability, and the presence of gaseous layers. Lauga et al. [6] also reviewed experimental, numerical and theoretical investigations on the subject of slip and pointed out the complex behaviour at a liquid/solid interface, involving an interplay of many physico-chemical parameters, including wetting conditions, shear rate, pressure, surface charge, surface roughness, impurities and dissolved gas. Slip is also observed in flows of rarefied gases in microtubes [8].

Navier [9] proposed a linear slip law according to which the slip velocity $u_w^*$, defined as the velocity of the fluid relative to that of the wall, is proportional to the wall shear stress, $\tau_w^*$. Thus,

$$\tau_w^* = \beta^* u_w^* \tag{1}$$

where $\beta^*$ is the slip coefficient, which varies in general with temperature, normal stress and pressure, molecular parameters, and the characteristics of the fluid/wall interface, e.g. the interaction between the fluid and the solid surface and surface roughness [10]. The limiting case of no slip is recovered for $\beta^* \to \infty$. It should

* Corresponding author.
*E-mail addresses:* skyrits@math.ntua.gr (S. Kyritsi-Yiallourou), georgios@ucy.ac.cy (G.C. Georgiou).

https://doi.org/10.1016/j.euromechflu.2018.05.002
0997-7546/

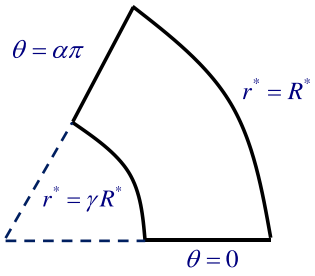


**Fig. 1.** Cross section of the tube.

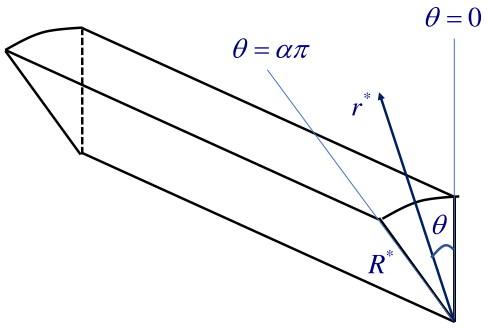


**Fig. 2.** Geometry when $\gamma = 0$ (the tube cross section is a circular section).

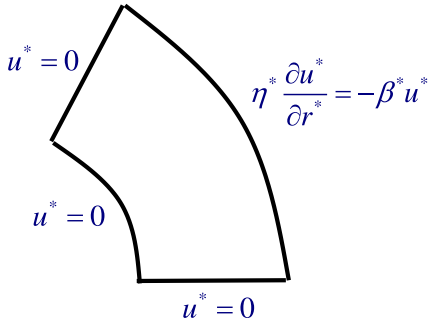


**Fig. 3.** Boundary conditions of the flow when Navier slip occurs only along the outer cylindrical wall.

be noted that starred symbols denote dimensional quantities and variables (symbols without stars correspond to dimensionless quantities).

The slip coefficient is related to the extrapolation length, $b^*$, which is defined as the characteristic length equal to the distance that the velocity profile at the wall must be extrapolated linearly to satisfy the no-slip boundary condition, by means of $\beta^* \equiv \eta^*/b^*$, where $\eta^*$ is the viscosity [11]. Recently, Bolaños and Vernescu [12] derived the Navier slip condition as the effective boundary condition in the limit of small roughness by combining homogenization methods and boundary-layer techniques and provided a formula for computing the slip length for various geometries and a theoretical justification for the observed slip in micro- and nano-fluidics.

Many different extensions of Navier's law have been proposed, the most important of which are the generalizations to power-law and dynamic slip equations. The reader is referred to the recent review of Hatzikiriakos [11] for more details.

Analytical solutions of Poiseuille flow with wall slip exist only for certain geometries including parallel plates, circular, annular, elliptic, equilateral triangular, and rectangular ducts [5,13–15]. Recently, Wang [5] considered the flow in an annular-sector duct with Navier slip along all walls. The solution of this flow problem in the no-slip case has been derived by Sparrow et al. [4]. Wang [5] derived a semi-analytical approximate solution using expansions of eigenfunctions in the radial direction and boundary collocation on the straight sides. The leading eigenvalues were calculated using perturbation theory and approximate formulas for the higher eigenvalues were used.

In the present work, we consider ducts the cross section of which is either a circular or an annular sector (see Figs. 1 and 2) and assume that Navier slip occurs only along the outer cylindrical wall. In other words, there is no slip along the straight sides and along the inner cylindrical wall in the case of an annular sector. It should be noted that this situation may arise if the material of construction or even the roughness of the outer cylindrical wall is different from those of the other walls of the duct (see, e.g., [7,10]). This flow is amenable to an exact analytical solution which is derived below for the sake of simplicity instead of the more general flow where slip occurs along both cylindrical walls with different slip coefficients. However, a brief derivation of the latter solution is also provided.

The governing equations are presented in Section 2. In Section 3, the analytical solution is derived and its form in various interesting special cases are also presented. The solution for the no-slip case is presented in Section 3.1. Results regarding the angle of the cross section, the radii ratio, and the slip coefficient are presented and discussed in Section 4. Finally, the conclusions of the present work are summarized in Section 5.

## 2. Governing equations

We consider the Poiseuille flow of a Newtonian fluid in an infinitely long horizontal duct the cross section of which is an annular sector defined by $\gamma R^* \le r^* \le R^*$ and $0 \le \theta \le \alpha\pi$, where $(r^*, \theta)$ are the polar coordinates, $R^*$ is the outer radius, $0 < \alpha < 2$, and $0 \le \gamma < 1$. The geometry is illustrated in Fig. 1. When $\gamma = 0$ the cross section is a circular sector, as illustrated in Fig. 2. If, for example, $\gamma = 0$ and $\alpha = 1$, the cross section is semicircular.

Assuming that the flow is unidirectional, driven by a constant pressure-gradient $(-dp^*/dz^*)$ in the absence of gravity, the $z$-component of the Navier–Stokes equation is simplified as follows

$$-\frac{dp^*}{dz^*} + \eta^*\left(\frac{\partial^2 u^*}{\partial r^{*2}} + \frac{1}{r^*}\frac{\partial u^*}{\partial r^*} + \frac{1}{r^{*2}}\frac{\partial^2 u^*}{\partial \theta^2}\right) = 0 \tag{2}$$

where $u^*$ is the axial velocity and the viscosity $\eta^*$ is constant (Newtonian fluid).

The boundary conditions of the flow are illustrated in Fig. 3. We assume that there is no-slip along the walls $\theta = 0$, $\theta = \alpha\pi$, and $r^* = \gamma R^*$. At the outer cylindrical wall, $r^* = R^*$, it is assumed that slip occurs following Navier's slip law. Given that $\tau_w^* = |\eta^* \partial u^*/\partial r^*|_{r^*=R^*}$, boundary condition (1) can be written as follows:

$$\eta^* \frac{\partial u^*}{\partial r^*}(R^*, \theta) + \beta^* u^*(R^*, \theta) = 0. \tag{3}$$

It should be noted that this condition is compatible with the no-slip boundary condition along the adjacent walls $\theta = 0$ and $\theta = \alpha\pi$.

It is preferable to work with dimensionless equations. We thus scale lengths by the outer radius of the tube, $R^*$, and the velocity by $(-dp^*/dz^*)R^{*2}/\eta^*$. Therefore, the dimensionless form of the flow problem is the following:

$$\left.\begin{aligned} \frac{\partial^2 u}{\partial r^2} + \frac{1}{r}\frac{\partial u}{\partial r} + \frac{1}{r^2}\frac{\partial^2 u}{\partial \theta^2} &= -1, 0 < r < 1, 0 < \theta < \alpha\pi \\ u(r, 0) = u(r, \alpha\pi) &= 0, 0 < r < 1 \\ u(\gamma, \theta) = \frac{\partial u}{\partial r}(1, \theta) + Bu(1, \theta) &= 0, 0 < \theta < \alpha\pi \end{aligned}\right\} \tag{4}$$

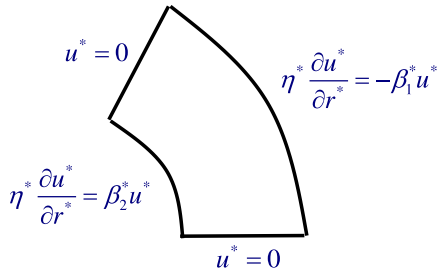


**Fig. 4.** Boundary conditions of the flow when Navier slip occurs along both cylindrical walls.

where $B$ is the slip number defined by

$$B \equiv \frac{\beta^*}{\eta^* R^*}. \tag{5}$$

Again, the no-slip case corresponds to $B \to \infty$.

## 3. Derivation of the solution

In order to use separation of variables we first need to homogenize the problem defined in (4). To that end we employ the transformation

$$u(r,\theta) = -f(\theta)r^2 + w(r,\theta). \tag{6}$$

It is easily verified that the partial differential equation $(4)_a$ and boundary conditions $(4)_b$ are satisfied when

$$f(\theta) = \frac{1}{2}\sin^2\theta - \frac{1}{4}\tan(\alpha\pi)\sin(2\theta). \tag{7}$$

Hence, the transformed problem reads:

$$\left.\begin{array}{c} \dfrac{\partial^2 w}{\partial r^2} + \dfrac{1}{r}\dfrac{\partial w}{\partial r} + \dfrac{1}{r^2}\dfrac{\partial^2 w}{\partial \theta^2} = 0, 0 < r < 1, 0 < \theta < \alpha\pi \\ w(r,0) = w(r,\alpha\pi) = 0, 0 < r < 1 \\ w(\gamma,\theta) = f(\theta)\gamma^2, 0 < \theta < \alpha\pi \\ \dfrac{\partial w}{\partial r}(1,\theta) + Bw(1,\theta) = (B+2)f(\theta), 0 < \theta < \alpha\pi \end{array}\right\}. \tag{8}$$

We now seek a separated solution of the form:

$$w(r,\theta) = \sum_{k=1}^{\infty} c_k(r)\varphi_k(\theta). \tag{9}$$

The Sturm–Liouville problem corresponding to problem (8) is the following [16]:

$$\left.\begin{array}{l} \phi''(\theta) = \lambda\phi(\theta), 0 < \theta < \alpha\pi \\ \phi(0) = \phi(\alpha\pi) = 0 \end{array}\right\}. \tag{10}$$

The eigenvalues and eigenfunctions of the above problem are:

$$\lambda_k = -\frac{k^2}{\alpha^2}, \quad \varphi_k(\theta) = \sqrt{\frac{2}{\alpha\pi}}\sin\left(\frac{k\theta}{\alpha}\right), \quad k = 1, 2, K. \tag{11}$$

Substituting into the PDE of Eq. (8) we get the Euler equation:

$$c_k''(r) + \frac{1}{r}c_k'(r) - \frac{k^2}{\alpha^2 r^2}c_k(r) = 0 \tag{12}$$

the solution of which is

$$c_k(r) = c_{1k}r^{-k/\alpha} + c_{2k}r^{k/\alpha}. \tag{13}$$

Therefore, for the satisfaction of boundary condition $(8)_c$ we require that

$$\sum_{k=1}^{\infty}\left(c_{1k}\gamma^{-k/\alpha} + c_{2k}\gamma^{k/\alpha}\right)\sin\left(\frac{k\theta}{\alpha}\right) = f(\theta)\gamma^2. \tag{14}$$

By multiplying Eq. (14) by $\sin(k\theta/\alpha)$ and integrating, one finds that

$$c_{1k}\gamma^{-k/\alpha} + c_{2k}\gamma^{k/\alpha} = \frac{2\gamma^2 I_k}{a\pi} \tag{15}$$

where $I_k$ is the Fourier coefficient of $f$:

$$I_k \equiv \int_0^{\alpha\pi} f(\theta)\sin\left(\frac{k\theta}{\alpha}\right)d\theta = -\frac{\alpha^3(1-\cos k\pi)}{k(k^2-4\alpha^2)}. \tag{16}$$

Therefore,

$$c_{1k} = \left(\frac{2\gamma^2 I_k}{a\pi} - c_{2k}\gamma^{k/\alpha}\right)\gamma^{k/\alpha} \tag{17}$$

and thus

$$w(r,\theta) = \sum_{k=1}^{\infty}\left[\left(\frac{2\gamma^2 I_k}{a\pi} - c_{2k}\gamma^{k/\alpha}\right)\gamma^{k/\alpha}r^{-k/\alpha} + c_{2k}r^{k/\alpha}\right] \times \sin\left(\frac{k\theta}{\alpha}\right). \tag{18}$$

The constant $c_{2k}$ is determined by applying the remaining boundary condition, i.e. the slip boundary condition $(8)_d$:

$$\sum_{k=1}^{\infty}\left[\left(B - \frac{k}{\alpha}\right)\left(\frac{2\gamma^2 I_k}{a\pi} - c_{2k}\gamma^{k/\alpha}\right)\gamma^{k/\alpha} + \left(B + \frac{k}{\alpha}\right)c_{2k}\right] \times \sin\left(\frac{k\theta}{\alpha}\right) = (B+2)f(\theta). \tag{19}$$

By means of the orthogonality of the eigenfunctions $\varphi_k$, we get:

$$\left(B - \frac{k}{\alpha}\right)\left(\frac{2\gamma^2 I_k}{a\pi} - c_{2k}\gamma^{k/\alpha}\right)\gamma^{k/\alpha} + \left(B + \frac{k}{\alpha}\right)c_{2k} = \frac{2(B+2)I_k}{\alpha\pi} \tag{20}$$

which gives:

$$c_{2k} = \frac{2I_k\left[B\left(1-\gamma^{k/\alpha+2}\right) + 2 + \frac{k}{\alpha}\gamma^{k/\alpha+2}\right]}{\alpha\pi\left[B\left(1-\gamma^{2k/\alpha}\right) + \frac{k}{\alpha}\left(1+\gamma^{2k/\alpha}\right)\right]}. \tag{21}$$

Substituting into Eq. (18) and rearranging we get Eq. (22) given in Box I. Therefore, the dimensionless velocity is given by Eq. (23) given in Box II. Eq. (23) is a special case of the solution of the more general flow where slip occurs along both cylindrical walls with different slip coefficients, which is given in Section 3.2. Some interesting special cases are considered below. The no-slip case ($B \to \infty$) is separately considered in Section 3.1. When $\gamma = 0$ (the cross section is a circular sector), Eq. (23) is simplified to

$$u(r,\theta) = \left[-\frac{1}{2}\sin^2\theta + \frac{1}{4}\tan(\alpha\pi)\sin(2\theta)\right]r^2 - \frac{2\alpha^2(B+2)}{\pi} \times \sum_{k=1}^{\infty}\frac{(1-\cos k\pi)r^{k/\alpha}}{k(k^2-4\alpha^2)(B+k/\alpha)}\sin\left(\frac{k\theta}{\alpha}\right). \tag{24}$$

When $\alpha = 1$, we get Eq. (25) given in Box III. Finally, when $\alpha = 1$ and $\gamma = 0$ (semicircular cross-section),

$$u(r,\theta) = -\frac{r^2}{2}\sin^2\theta - \frac{2(B+2)}{\pi}\sum_{k=1}^{\infty}\frac{(1-\cos k\pi)r^k\sin(k\theta)}{k(k^2-4)(B+k)} \tag{26}$$

or

$$u(r,\theta) = -\frac{1}{2}\sin^2\theta\, r^2 - \frac{4(B+2)}{\pi} \times \sum_{i=1}^{\infty}\frac{r^{2i-1}\sin[(2i-1)\theta]}{(2i-3)(2i-1)(2i+1)(B+2i-1)}. \tag{27}$$

As for the volumetric flow rate,

$$Q \equiv \int_0^{\alpha\pi}\int_{\gamma}^{1} u(r,\theta)r\,dr\,d\theta \tag{28}$$

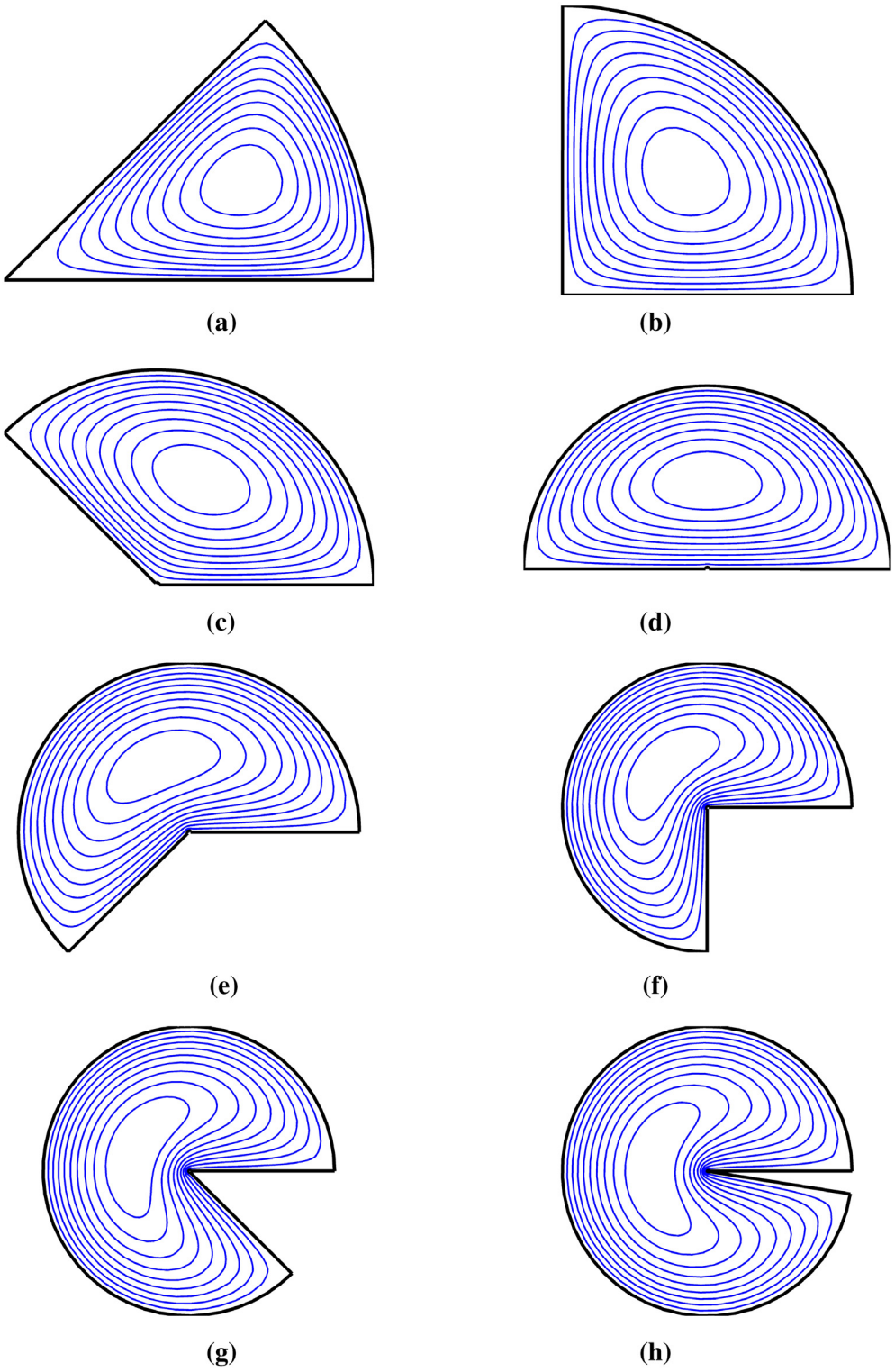


**Fig. 5.** Velocity contours in the case of no slip for $\gamma = 0$ and various values of $\alpha$: (a) $\alpha = 0.25$; (b) $\alpha = 0.5$; (c) $\alpha = 0.75$; (d) $\alpha = 1$; (e) $\alpha = 1.25$; (f) $\alpha = 1.5$; (g) $\alpha = 1.75$; (h) $\alpha = 1.95$.

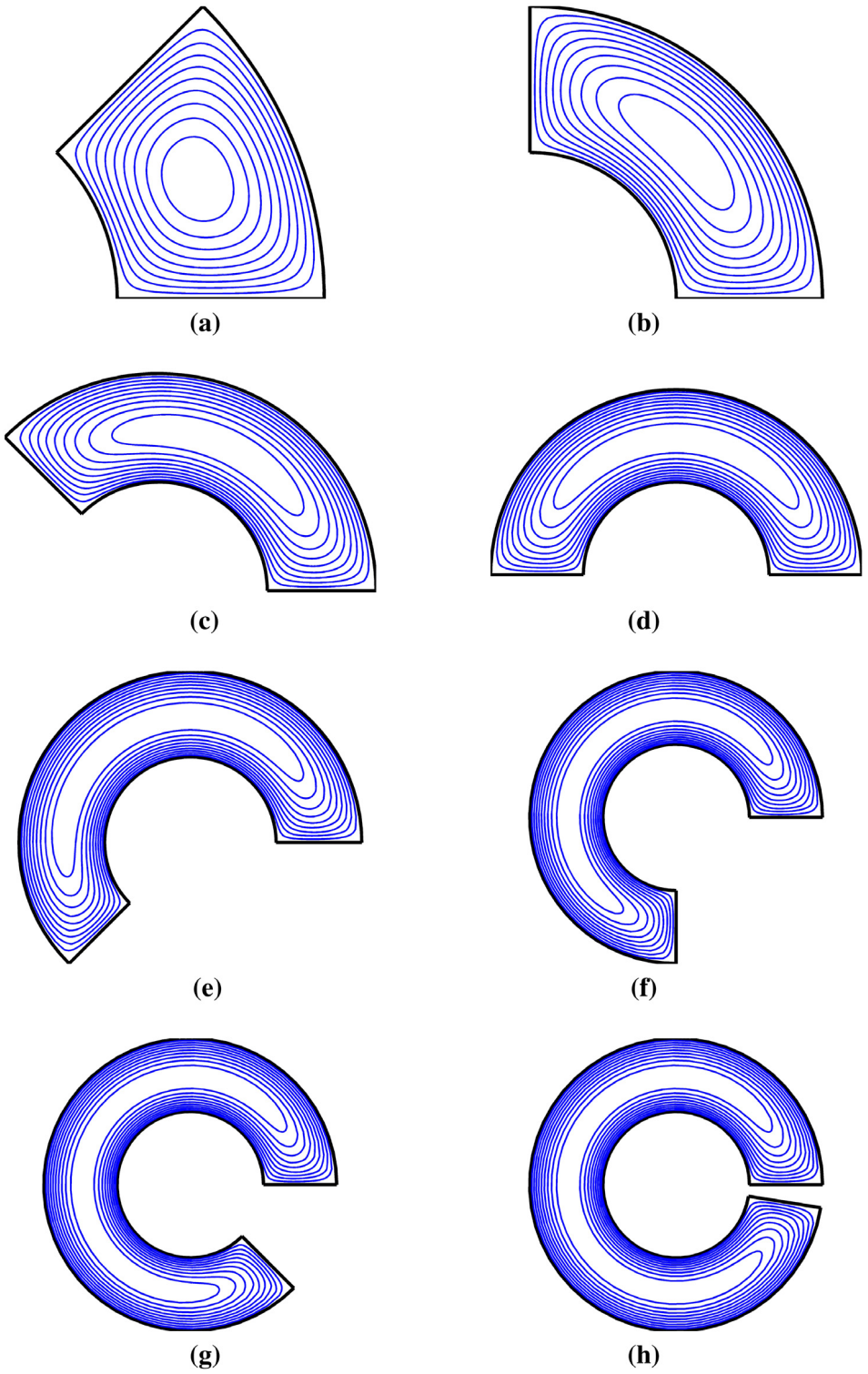


**Fig. 6.** Velocity contours in the case of no slip for $\gamma = 0.5$ and various values of $\alpha$: (a) $\alpha = 0.25$; (b) $\alpha = 0.5$; (c) $\alpha = 0.75$; (d) $\alpha = 1$; (e) $\alpha = 1.25$; (f) $\alpha = 1.5$; (g) $\alpha = 1.75$; (h) $\alpha = 1.95$.

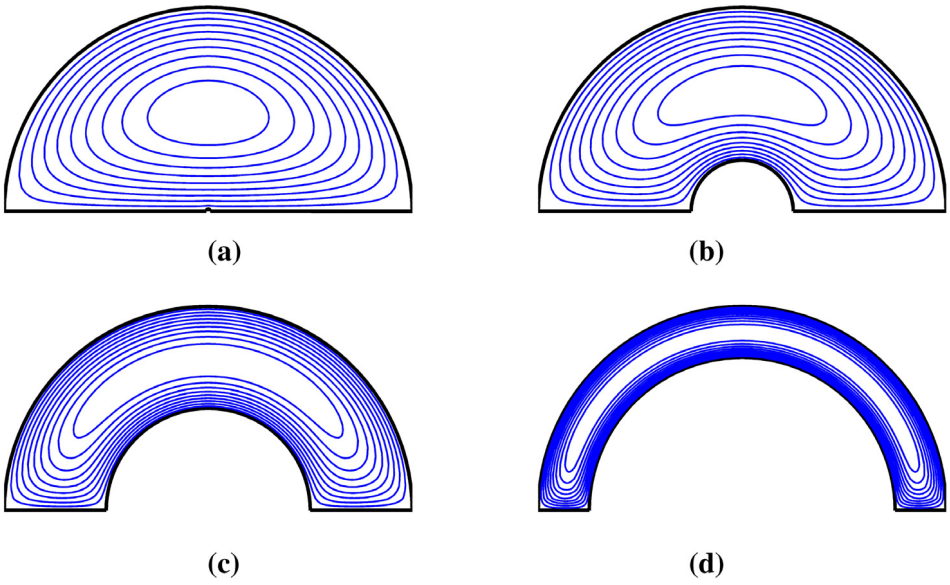


**Fig. 7.** Velocity contours in the case of no slip for $\alpha = 1$ and various values of $\gamma$: (a) $\gamma = 0$; (b) $\gamma = 0.25$; ( c) $\gamma = 0.5$; (d) $\gamma = 0.75$.

$$w(r,\theta) = \frac{2}{\alpha\pi}\sum_{k=1}^{\infty} \frac{I_k \left\{\left[B\left(1-\gamma^{k/\alpha-2}\right)+\frac{k}{\alpha}-2\gamma^{k/\alpha-2}\right]\gamma^{k/\alpha+2} r^{-k/\alpha} + \left[B\left(1-\gamma^{k/\alpha+2}\right)+2+\frac{k}{\alpha}\gamma^{k/\alpha+2}\right] r^{k/\alpha}\right\}}{B\left(1-\gamma^{2k/\alpha}\right)+\frac{k}{\alpha}\left(1+\gamma^{2k/\alpha}\right)} \sin\left(\frac{k\theta}{\alpha}\right). \tag{22}$$

**Box I.**

$$u(r,\theta) = \left[-\frac{1}{2}\sin^2\theta + \frac{1}{4}\tan(\alpha\pi)\sin(2\theta)\right] r^2 - \frac{2\alpha^2}{\pi}\sum_{k=1}^{\infty}\frac{1-\cos(k\pi)}{k(k^2-4\alpha^2)}\times \frac{\left\{\left[B\left(1-\gamma^{k/\alpha-2}\right)+\frac{k}{\alpha}-2\gamma^{k/\alpha-2}\right]\gamma^{k/\alpha+2} r^{-k/\alpha} + \left[B\left(1-\gamma^{k/\alpha+2}\right)+2+\frac{k}{\alpha}\gamma^{k/\alpha+2}\right] r^{k/\alpha}\right\}}{B\left(1-\gamma^{2k/\alpha}\right)+\frac{k}{\alpha}\left(1+\gamma^{2k/\alpha}\right)} \sin\left(\frac{k\theta}{\alpha}\right). \tag{23}$$

**Box II.**

one gets

$$\begin{aligned} Q \;=\; & \frac{1}{16}\left(\tan\alpha\pi-\alpha\pi\right)\left(1-\gamma^4\right)+\frac{2\alpha^4}{\pi} \\ & \times\sum_{k=1}^{\infty}\frac{(1-\cos k\pi)^2}{k^2(k^2-4\alpha^2)^2\left[B(1-\gamma^{2k/\alpha})+k(1+\gamma^{2k/\alpha})/\alpha\right]}\times \\ & \left\{(k+2\alpha)\left[B\left(2\gamma^{k/\alpha+2}-\gamma^{2k/\alpha}-\gamma^4\right)\right.\right. \\ & \left.+\left(k/\alpha+2\right)\gamma^{k/\alpha+2}-k\gamma^4/\alpha-2\gamma^{2k/\alpha}\right] \\ & -(k-2\alpha)\left[B(1-\gamma^{k/\alpha+2})+2+k\gamma^{k/\alpha+2}/\alpha\right] \\ & \left.(1-\gamma^{k/\alpha+2})\right\}. \end{aligned} \tag{29}$$

When $\gamma = 0$,

$$\begin{aligned} Q \;=\; & \frac{1}{16}\left(\tan\alpha\pi-\alpha\pi\right)-\frac{2\alpha^4(B+2)}{\pi} \\ & \times\sum_{k=1}^{\infty}\frac{(1-\cos k\pi)^2}{k^2(k+2\alpha)^2(k-2\alpha)(B+k/\alpha)} \end{aligned} \tag{30}$$

and when $\alpha = 1$

$$\begin{aligned} Q \;=\; & -\frac{\pi}{16}\left(1-\gamma^4\right) \\ & +\frac{2}{\pi}\sum_{k=1}^{\infty}\frac{(1-\cos k\pi)^2}{k^2(k^2-4)^2\left[B(1-\gamma^{2k})+k(1+\gamma^{2k})\right]}\times \\ & \left\{(k+2)\left[B\left(2\gamma^{k+2}-\gamma^{2k}-\gamma^4\right)\right.\right. \\ & \left.+(k+2)\,\gamma^{k+2}-k\gamma^4-2\gamma^{2k}\right] \\ & \left.-(k-2)\left[B(1-\gamma^{k+2})+2+k\gamma^{k+2}\right](1-\gamma^{k+2})\right\}. \end{aligned} \tag{31}$$

When $\alpha = 1$ and $\gamma = 0$ (semicircular cross-section),

$$Q = -\frac{\pi}{16}-\frac{2(B+2)}{\pi}\sum_{k=1}^{\infty}\frac{(1-\cos k\pi)^2}{k^2(k+2)^2(k-2)(B+k)} \tag{32}$$

or

$$\begin{aligned} Q \;=\; & -\frac{\pi}{16}-\frac{8(B+2)}{\pi} \\ & \times\sum_{i=1}^{\infty}\frac{1}{(2i-1)^2(2i+1)^2(2i-3)(B+2i-1)}. \end{aligned} \tag{33}$$

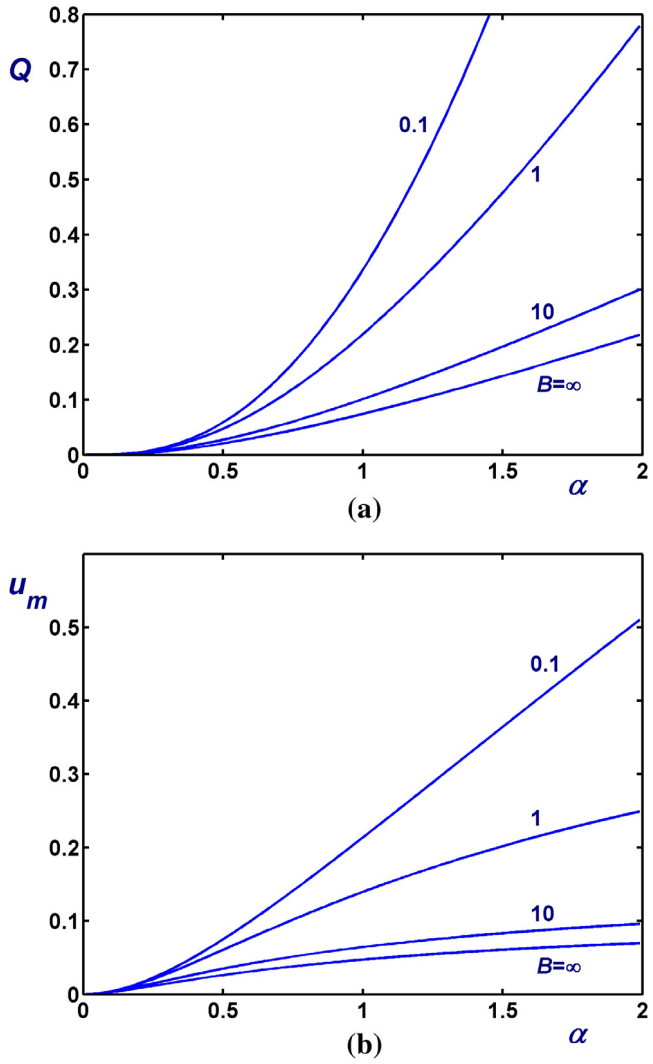


**Fig. 8.** Volumetric flow rate (a) and mean velocity (b) versus $\alpha$ for $\gamma = 0$ and various values of the slip number.

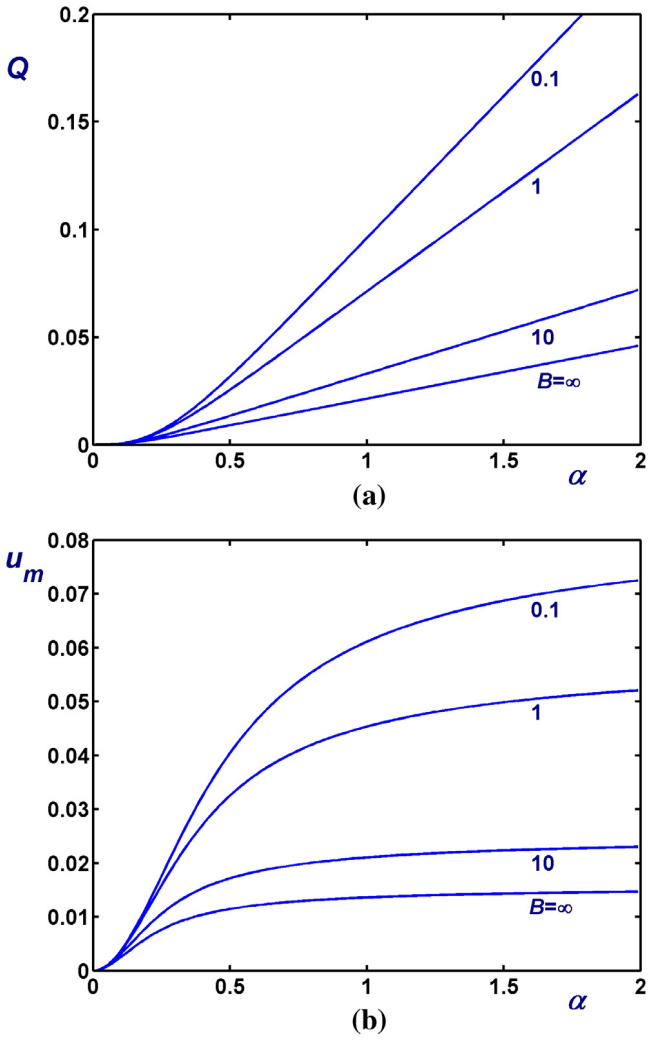


**Fig. 9.** Volumetric flow rate (a) and mean velocity (b) versus $\alpha$for $\gamma = 0.5$ and various values of the slip number.

### 3.1. The no-slip case

In this subsection, some special solutions for the no-slip case are provided for convenience. When $B \to \infty$, Eq. (23) is reduced to

$$\begin{aligned} u(r,\theta) = &\left[-\frac{1}{2}\sin^2\theta + \frac{1}{4}\tan(\alpha\pi)\sin(2\theta)\right] r^2 \\ &- \frac{2\alpha^2}{\pi}\sum_{k=1}^{\infty} \frac{1-\cos(k\pi)}{k(k^2-4\alpha^2)(1-\gamma^{2k/\alpha})} \\ &\times \left[\left(1-\gamma^{k/\alpha-2}\right)\gamma^{k/\alpha+2}\right. \\ &\left.\times\, r^{-k/\alpha} + \left(1-\gamma^{k/\alpha+2}\right) r^{k/\alpha}\right] \sin\left(\frac{k\theta}{\alpha}\right) \end{aligned} \tag{34}$$

and the volumetric flow rate is given by

$$\begin{aligned} Q = &\frac{1}{16}\left(\tan\alpha\pi - \alpha\pi\right)\left(1-\gamma^4\right) \\ &+ \frac{2\alpha^4}{\pi}\sum_{k=1}^{\infty} \frac{(1-\cos k\pi)^2}{k^2(k^2-4\alpha^2)^2(1-\gamma^{2k/\alpha})} \\ &\times \left[(k+2\alpha)\left(2\gamma^{k/\alpha+2} - \gamma^{2k/\alpha} - \gamma^4\right)\right. \\ &\left.-(k-2\alpha)\left(1-\gamma^{k/\alpha+2}\right)^2\right]. \end{aligned} \tag{35}$$

Although equivalent, the above expressions are considerably simpler than the expressions derived by Sparrow et al. [4], who were the first to solve the Poiseuille flow in an annular-sector duct with no slip along the walls. The latter authors introduced a coordinate transformation to map the annular sector into a rectangular region which simplifies the mathematical problem but results in a longer expansion, the convergence of which is extremely slow.

When $\gamma = 0$, Eq. (34) is simplified as follows:

$$\begin{aligned} u(r,\theta) = &\left[-\frac{1}{2}\sin^2\theta + \frac{1}{4}\tan(\alpha\pi)\sin(2\theta)\right] r^2 \\ &- \frac{2\alpha^2}{\pi}\sum_{k=1}^{\infty} \frac{1-\cos(k\pi)}{k(k^2-4\alpha^2)} r^{k/\alpha} \sin\left(\frac{k\theta}{\alpha}\right) \end{aligned} \tag{36}$$

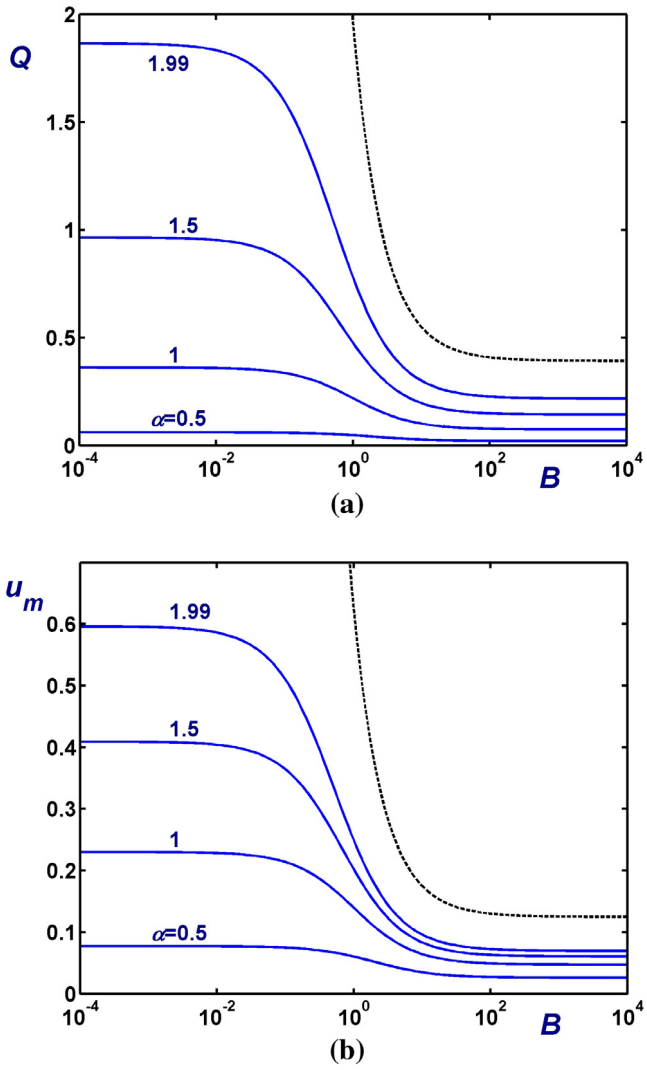


**Fig. 10.** Volumetric flow rate (a) and mean velocity (b) versus the slip number $B$ for $\gamma = 0$ and various values of $\alpha$. The dashed line corresponds to the axisymmetric Poiseuille flow with slip at the wall.

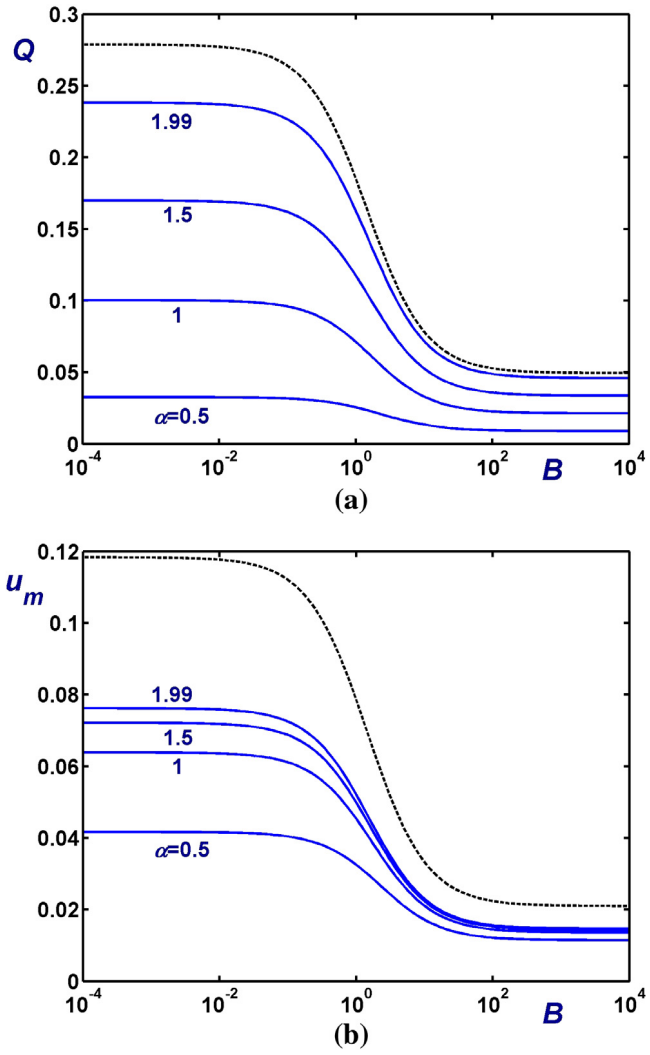


**Fig. 11.** Volumetric flow rate (a) and mean velocity (b) versus the slip number $B$ for $\gamma = 0.5$ and various values of $\alpha$. The dashed line corresponds to the axisymmetric annular Poiseuille flow with slip along the outer cylinder and no-slip along the inner one.

and

$$Q = \frac{1}{16}(\tan\alpha\pi - \alpha\pi) - \frac{2\alpha^4}{\pi}\sum_{k=1}^{\infty}\frac{(1-\cos k\pi)^2}{k^2(k+2\alpha)^2(k-2\alpha)}. \tag{37}$$

For $\alpha = 1$, we get:

$$u(r,\theta) = -\frac{1}{2}\sin^2\theta\, r^2 - \frac{2}{\pi}\sum_{k=1}^{\infty}\frac{1-\cos(k\pi)}{k(k^2-4)(1-\gamma^{2k})} \times \left[\left(1-\gamma^{k-2}\right)\gamma^{k+2}r^{-k} + \left(1-\gamma^{k+2}\right)r^k\right]\sin(k\theta) \tag{38}$$

and

$$Q = -\frac{\pi}{16}\left(1-\gamma^4\right) + \frac{2}{\pi}\sum_{k=1}^{\infty}\frac{(1-\cos k\pi)^2}{k^2(k^2-4)^2(1-\gamma^{2k})} \times \left[(k+2)\left(2\gamma^{k+2} - \gamma^{2k} - \gamma^4\right) - (k-2)\left(1-\gamma^{k+2}\right)^2\right]. \tag{39}$$

Finally, when $\alpha = 1$ and $\gamma = 0$ (semicircular cross-section),

$$u(r,\theta) = -\frac{1}{2}\sin^2\theta\, r^2 - \frac{2}{\pi}\sum_{k=1}^{\infty}\frac{1-\cos(k\pi)}{k(k^2-4)}r^k\sin(k\theta) \tag{40}$$

or

$$u(r,\theta) = -\frac{1}{2}\sin^2\theta\, r^2 - \frac{4}{\pi}\sum_{i=1}^{\infty}\frac{r^{2i-1}\sin[(2i-1)\theta]}{(2i-3)(2i-1)(2i+1)}. \tag{41}$$

The latter solution has also been derived by Alassar [17]. The volumetric flow rate is given by

$$Q = -\frac{\pi}{16} - \frac{2}{\pi}\sum_{k=1}^{\infty}\frac{(1-\cos k\pi)^2}{k^2(k+2)^2(k-2)} \tag{42}$$

or

$$Q = -\frac{\pi}{16} - \frac{8}{\pi}\sum_{i=1}^{\infty}\frac{1}{(2i-1)^2(2i+1)^2(2i-3)}. \tag{43}$$

By means of partial fractions, it can then be shown that $Q = \pi/8 - 1/\pi$, a result also reported in [15].

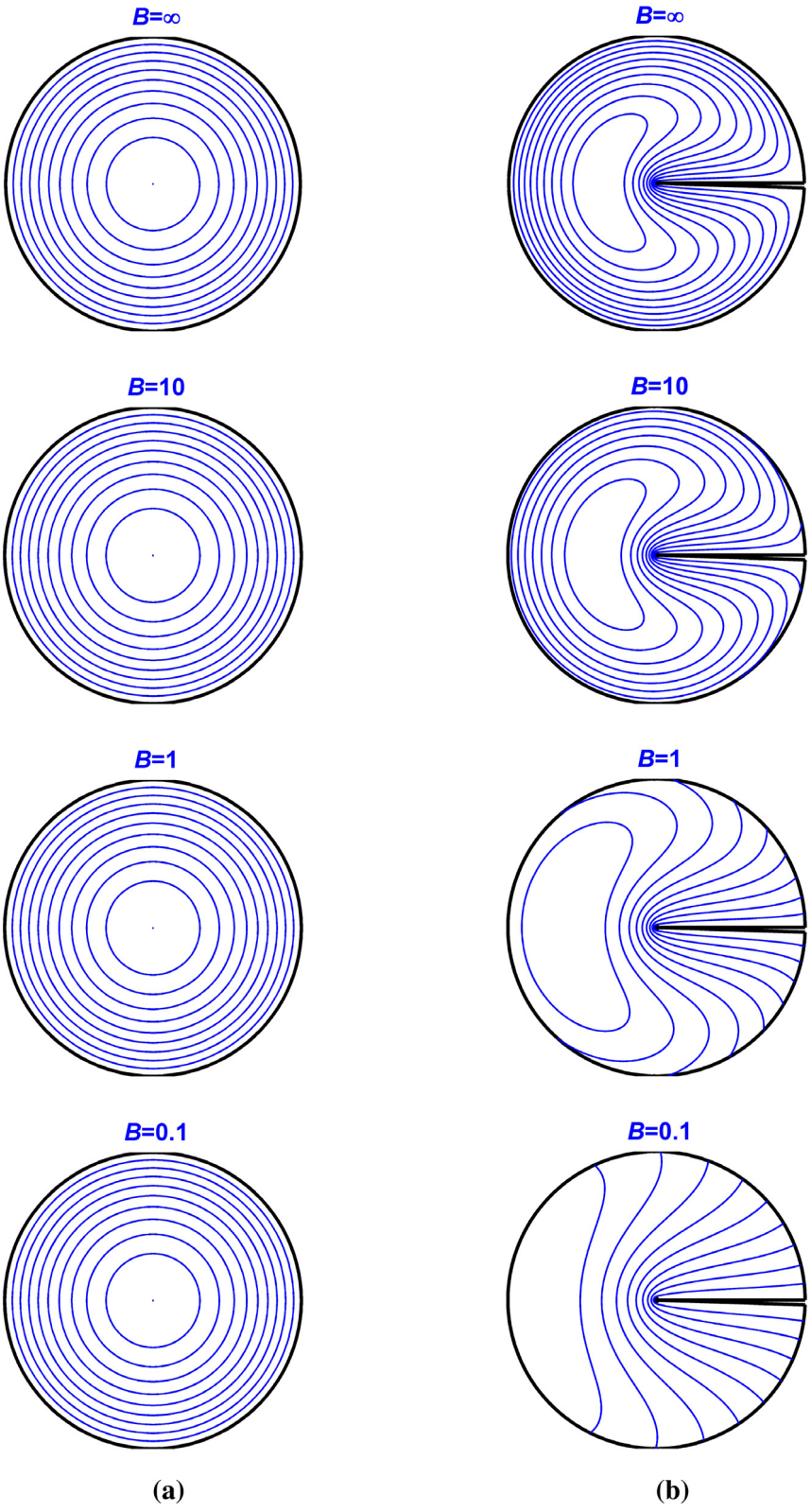


**Fig. 12.** Velocity contours for various values of the slip number: (a) axisymmetric Poiseuille flow; (b) flow in a tube with $\alpha = 1.99$ and $\gamma = 0$.

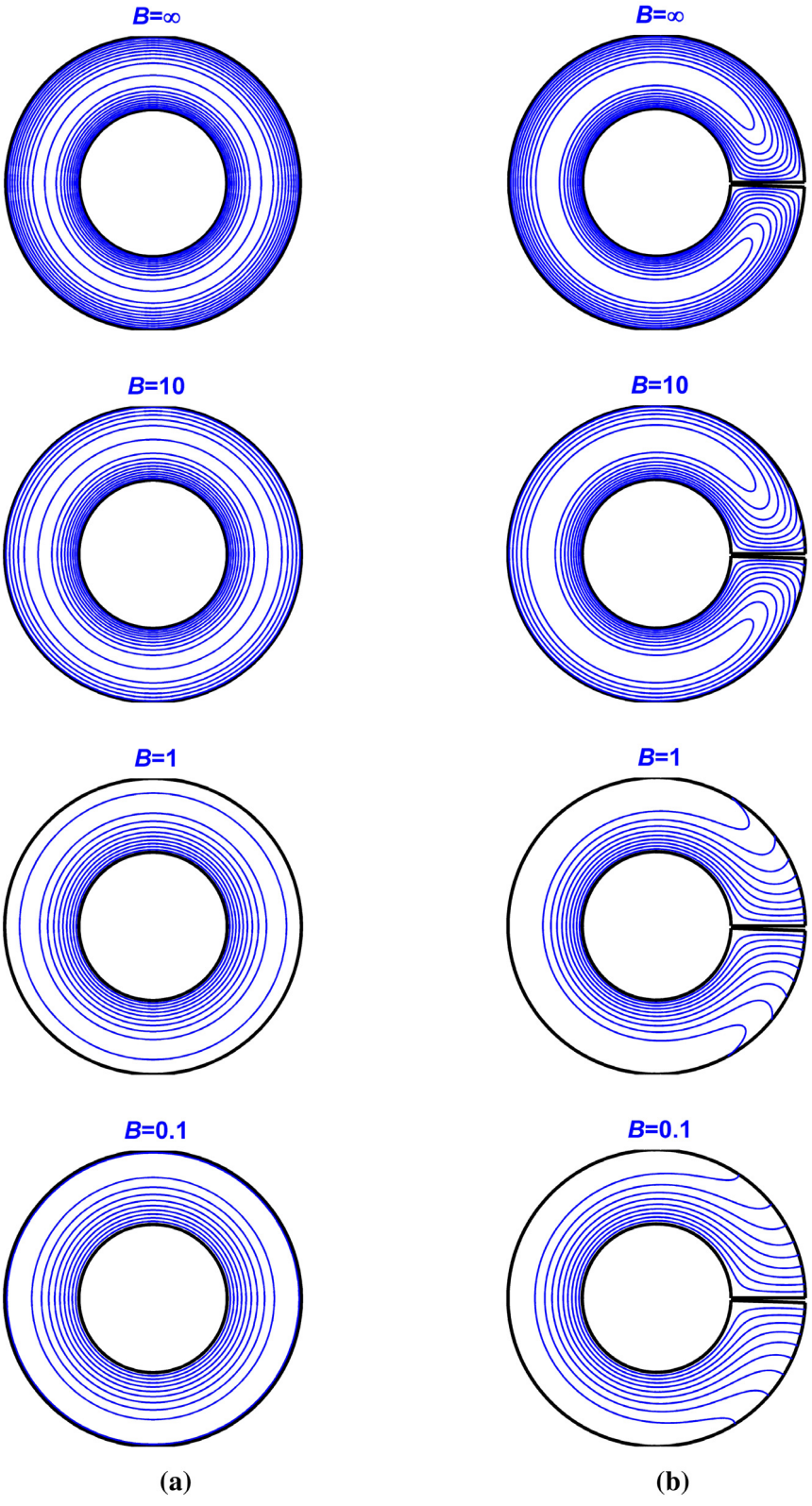


**Fig. 13.** Velocity contours for various values of the slip number: (a) annular Poiseuille flow with $\gamma = 0.5$; (b) flow in a tube with $\alpha = 1.99$ and $\gamma = 0.5$.

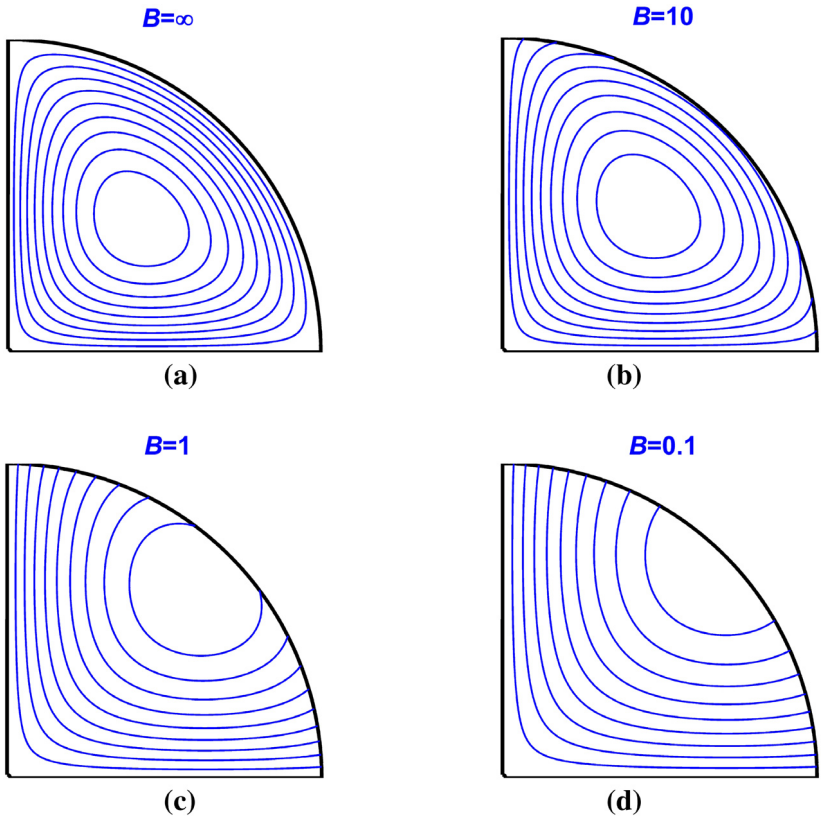


**Fig. 14.** Velocity contours for $\alpha = 0.5$, $\gamma = 0$ and various values of the slip number $B$: (a) $B = \infty$ (no slip); (b) $B = 10$ (weak slip); (c) $B = 1$ (moderate slip); (d) $B = 0.1$ (strong slip).

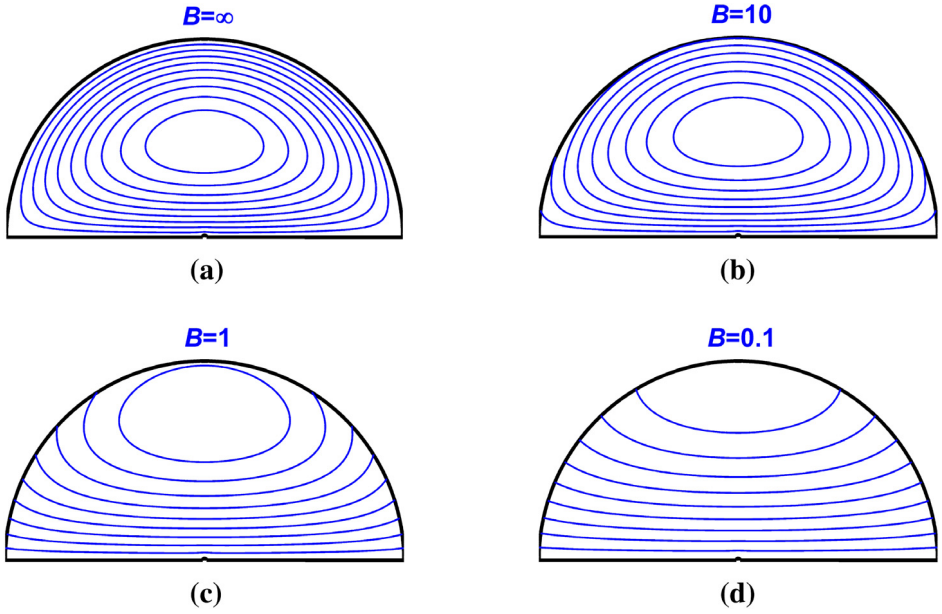


**Fig. 15.** Velocity contours for $\alpha = 1$, $\gamma = 0$ and various values of the slip number $B$: (a) $B = \infty$ (no slip); (b) $B = 10$ (weak slip); (c) $B = 1$ (moderate slip); (d) $B = 0.1$ (strong slip).

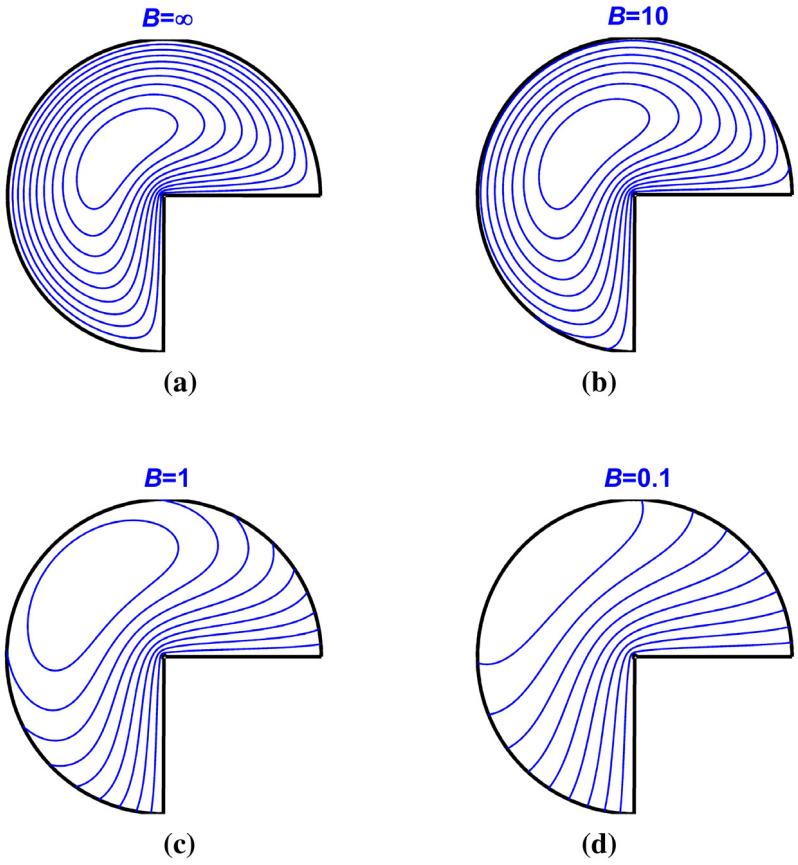


**Fig. 16.** Velocity contours for $\alpha = 1.5$, $\gamma = 0$ and various values of the slip number $B$: (a) $B = \infty$ (no slip); (b) $B = 10$ (weak slip); (c) $B = 1$ (moderate slip); (d) $B = 0.1$ (strong slip).

### 3.2. The solution when non-uniform slip occurs along both cylindrical walls

In this subsection, we consider the more general flow where Navier slip is allowed to occur along both the cylindrical walls with different slip coefficients, $\beta_1^*$ along the outer wall and $\beta_2^*$ along the inner one ($\gamma > 0$), as illustrated in Fig. 4.

Using the same scales as before, the dimensionless flow problem to be solved is:

$$\left.\begin{aligned} &\frac{\partial^2 u}{\partial r^2} + \frac{1}{r}\frac{\partial u}{\partial r} + \frac{1}{r^2}\frac{\partial^2 u}{\partial \theta^2} = -1,\ 0 < r < 1,\ 0 < \theta < \alpha\pi \\ &u(r,0) = u(r,\alpha\pi) = 0,\ 0 < r < 1 \\ &\frac{\partial u}{\partial r}(\gamma,\theta) - B_2 u(\gamma,\theta) = 0,\ 0 < \theta < \alpha\pi \\ &\frac{\partial u}{\partial r}(1,\theta) + B_1 u(1,\theta) = 0,\ 0 < \theta < \alpha\pi \end{aligned}\right\} \tag{44}$$

where the two slip numbers are defined by $B_i \equiv \beta_i^*/(\eta^* R^*)$, $i = 1, 2$. It should be noted that when $B_2 \to \infty$ the flow studied in the main paper is recovered. If instead $B_1 \to \infty$, the solution where slip occurs only along the inner cylindrical wall is obtained. Finally, by setting $B_1 = B_2 = B$, the same slip law is applied along both the walls.

Following the same steps as above we find the following expression for $w(r,\theta)$:

$$w(r,\theta) = \sum_{k=1}^{\infty}\left[\frac{\frac{2}{a\pi}(B_2\gamma - 2)\gamma I_k - \left(B_2 - \frac{k}{\alpha\gamma}\right)\gamma^{k/\alpha}c_{2k}}{B_2 + \frac{k}{\alpha\gamma}} \times \gamma^{k/\alpha}r^{-k/\alpha} + c_{2k}r^{k/\alpha}\right]\sin\left(\frac{k\theta}{\alpha}\right) \tag{45}$$

where

$$c_{2k} = \frac{2I_k\left\{B_1\left[1 - \frac{(B_2\gamma-2)}{(B_2\gamma+k/\alpha)}\gamma^{k/\alpha+2}\right] + 2 + \frac{k}{\alpha}\frac{(B_2\gamma-2)}{(B_2\gamma+k/\alpha)}\gamma^{k/\alpha+2}\right\}}{\alpha\pi\left\{B_1\left[1 - \frac{(B_2\gamma-k/\alpha)}{(B_2\gamma+k/\alpha)}\gamma^{2k/\alpha}\right] + \frac{k}{\alpha}\left[1 + \frac{(B_2\gamma-k/\alpha)}{(B_2\gamma+k/\alpha)}\gamma^{2k/\alpha}\right]\right\}}. \tag{46}$$

Substituting Eq. (46) into Eq. (45) and simplifying we get Eq. (47) given in Box IV. Therefore, the dimensionless velocity is given by Eq. (48) given in Box V. It is readily verified that if $B_2 \to \infty$ then Eq. (23) is recovered. If instead $B_1 \to \infty$ (no slip along the outer cylindrical wall), we have:

$$\begin{aligned} u(r,\theta) = &\left[-\frac{1}{2}\sin^2\theta + \frac{1}{4}\tan(\alpha\pi)\sin(2\theta)\right]r^2 \\ &- \frac{2\alpha^2}{\pi}\sum_{k=1}^{\infty}\frac{[1-\cos(k\pi)]\sin(k\theta/\alpha)}{k(k^2-4\alpha^2)\left(1 - \frac{B_2\gamma-k/\alpha}{B_2\gamma+k/\alpha}\gamma^{2k/\alpha}\right)} \times \\ &\left[\frac{B_2\gamma\left(1-\gamma^{k/\alpha-2}\right) - 2 + \frac{k}{\alpha}\gamma^{k/\alpha-2}}{B_2\gamma + k/\alpha}\gamma^{k/\alpha+2}r^{-k/\alpha} + \left(1 - \frac{B_2\gamma - 2}{B_2\gamma + k/\alpha}\gamma^{k/\alpha+2}\right)r^{k/\alpha}\right]. \end{aligned} \tag{49}$$

$$u(r,\theta) = -\frac{r^2}{2}\sin^2\theta - \frac{2}{\pi}\sum_{k=1}^{\infty}\frac{1-\cos(k\pi)}{k(k^2-4)}\times \frac{\left\{\left[B\left(1-\gamma^{k-2}\right)+k-2\gamma^{k-2}\right]\gamma^{k+2}r^{-k}+\left[B\left(1-\gamma^{k+2}\right)+2+k\gamma^{k+2}\right]r^{k}\right\}}{B\left(1-\gamma^{2k}\right)+k\left(1+\gamma^{2k}\right)}\sin(k\theta)\,. \tag{25}$$

**Box III.**

$$w(r,\theta) = \frac{2}{\alpha\pi}\sum_{k=1}^{\infty}\frac{I_k\sin(k\theta/\alpha)}{B_1\left(1-\frac{B_2\gamma-k/\alpha}{B_2\gamma+k/\alpha}\gamma^{2k/\alpha}\right)+\frac{k}{\alpha}\left(1+\frac{B_2\gamma-k/\alpha}{B_2\gamma+k/\alpha}\gamma^{2k/\alpha}\right)}\times \left\{\frac{B_2\gamma\left[B_1\left(1-\gamma^{k/\alpha-2}\right)+\frac{k}{\alpha}-2\gamma^{k/\alpha-2}\right]-2\left(B_1+\frac{k}{\alpha}\right)+\frac{k}{\alpha}(B_1+2)\gamma^{k/\alpha-2}}{B_2\gamma+k/\alpha}\gamma^{k/\alpha+2}r^{-k/\alpha} + \left[B_1\left(1-\frac{B_2\gamma-2}{B_2\gamma+k/\alpha}\gamma^{k/\alpha+2}\right)+2+\frac{k(B_2\gamma-2)}{\alpha(B_2\gamma+k/\alpha)}\gamma^{k/\alpha+2}\right]r^{k/\alpha}\right\}. \tag{47}$$

**Box IV.**

$$u(r,\theta) = \left[-\frac{1}{2}\sin^2\theta+\frac{1}{4}\tan(\alpha\pi)\sin(2\theta)\right]r^2 - \frac{2\alpha^2}{\pi}\sum_{k=1}^{\infty}\frac{[1-\cos(k\pi)]\sin(k\theta/\alpha)}{k(k^2-4\alpha^2)\left[B_1\left(1-\frac{B_2\gamma-k/\alpha}{B_2\gamma+k/\alpha}\gamma^{2k/\alpha}\right)+\frac{k}{\alpha}\left(1+\frac{B_2\gamma-k/\alpha}{B_2\gamma+k/\alpha}\gamma^{2k/\alpha}\right)\right]}\times \left\{\frac{B_2\gamma\left[B_1\left(1-\gamma^{k/\alpha-2}\right)+\frac{k}{\alpha}-2\gamma^{k/\alpha-2}\right]-2\left(B_1+\frac{k}{\alpha}\right)+\frac{k}{\alpha}(B_1+2)\gamma^{k/\alpha-2}}{B_2\gamma+k/\alpha}\gamma^{k/\alpha+2}r^{-k/\alpha} + \left[B_1\left(1-\frac{B_2\gamma-2}{B_2\gamma+k/\alpha}\gamma^{k/\alpha+2}\right)+2+\frac{k(B_2\gamma-2)}{\alpha(B_2\gamma+k/\alpha)}\gamma^{k/\alpha+2}\right]r^{k/\alpha}\right\}. \tag{48}$$

**Box V.**

All terms involving the slip number $B_2$ vanish when $\gamma = 0$ to yield the classical no-slip solution for the circular-sector duct.

## 4. Results and discussion

We first consider the case of no-slip along all walls. Representative results are illustrated in Figs. 5–7. In Figs. 5 and 6, the velocity contours for respectively $\gamma = 0$ (circular sector) and 0.5 (annular sector) are plotted for various values of $\alpha$. In Fig. 7, we plotted the velocity contours for a fixed angle ($\alpha = 1$) and various values of $\gamma$. It should be noted that in all the contour figures of this paper, 9 equidistant contours (ranging from $0.1u_{\max}$ to $0.9u_{\max}$, $u_{\max}$ being the maximum velocity) are plotted.

The volumetric flow rate increases as $\alpha$ is increased or as $\gamma$ is reduced, as expected. The effect of the angle parameter $\alpha$ in the case the cross section is a circular sector ($\gamma = 0$) can be seen in Fig. 8, where the volumetric flow rate $Q$ and the mean (cross-sectionally averaged) velocity, defined by

$$u_m \equiv \frac{Q}{\alpha\pi(1-\gamma^2)/2} \tag{50}$$

are plotted for four values of the slip number B, corresponding to no ($B = \infty$), weak ($B = 10$), moderate ($B = 1$), and strong ($B = 0.1$) slip. As expected, the volumetric flow rate and the mean velocity increase with slip and with the opening angle parameter $\alpha$. We have also compared the volumetric flow rates in the case of no-slip ($B = \infty$) in both Figs. 8 and 9 with the analytical solution derived by Sparrow et al. [4]. The two solutions are equivalent but the convergence of the latter is very slow, e.g. for a 6-significant-digit accuracy up to 10000 terms may be needed instead of around 50.

Similar results have been obtained for the case where the cross-section of the duct is an annular sector; as an example, Fig. 9 shows results with $\gamma = 0.5$. In this case, however, the volumetric flow rate and the mean velocity are much lower than their counterparts for $\gamma = 0$.

The effect of slip on the volumetric flow rate and the mean velocity is illustrated in Figs. 10 and 11 for $\gamma = 0$ (circular sector) and $\gamma = 0.5$ (annular sector), respectively, and various values of the angle parameter $\alpha$. Again both $Q$ and $u_m$increase as $\alpha$ is increased or as slip is enhanced. As slip becomes stronger, both quantities tend to an asymptotic value reaching a plateau. This is not the case with the classical axisymmetric Poiseuille flow where there is no inner cylindrical wall. In this case, the velocity and the volumetric flow rate are given by

$$u = \frac{1}{4}\left(1+\frac{2}{B}-r^2\right) \tag{51}$$

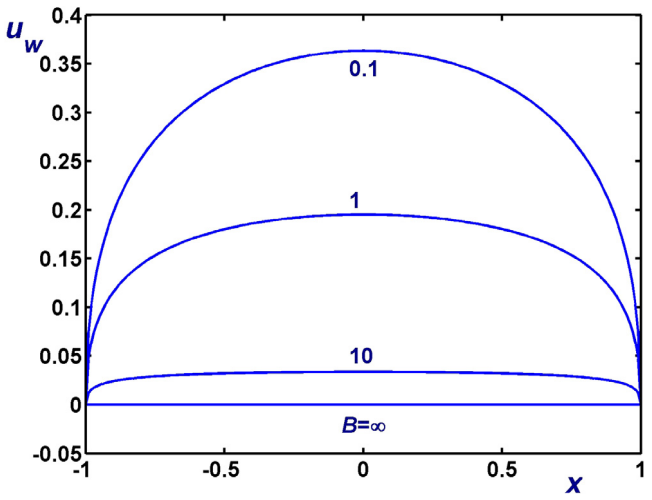


**Fig. 17.** Slip velocity for $\alpha = 1$, $\gamma = 0$ and various values of the slip number $B$.

and

$$Q = \frac{\pi}{8}\left(1 + \frac{4}{B}\right). \tag{52}$$

It is clear that in the limit of infinite slip ($B \to 0$), the volumetric flow rate also becomes infinite and the velocity becomes uniform. The dashed lines in Fig. 10 correspond to the axisymmetric Poiseuille flow. Comparing the velocity contours of the axisymmetric Poiseuille flow with the results for a circular sector with $\alpha = 1.99$ (i.e. for almost full circle) in Fig. 12 is instructive. The velocity contours of the axisymmetric Poiseuille flow look the same but they actually correspond to different velocity values in the interval $[1/(2B),\ 1/4 + 1/(2B)]$. It is clear that the difference between the minimum and maximum values of the velocity is constant which explains the fact that the velocity contours look identical. In the case of the circular sector (Fig. 12b) the minimum velocity is zero due to the no-slip boundary condition on parts of the boundary and the maximum velocity, which occurs at an angle $\theta = a\pi/2$ due to symmetry, moves towards the outer wall as slip is enhanced. In the limit of infinite slip the maximum velocity coincides with the maximum slip velocity.

The results in Fig. 11 for the case of an annular sector with $\gamma = 0.5$ are similar, with the volumetric flow rate and the mean velocity being much lower. The dashed lines correspond to the axisymmetric annular Poiseuille flow with slip along the outer cylinder and no-slip along the inner cylinder. The velocity and the volumetric flow rate in this case are given by

$$u = -\frac{1}{4}\left(r^2 - \gamma^2\right) + \frac{B(1-\gamma^2)+2}{4\left[1 + B\ln(1/\gamma)\right]}\ln\left(\frac{r}{\gamma}\right) \tag{53}$$

and

$$Q = \frac{\pi}{8}\left\{\frac{B(1-\gamma^2)+2}{1+B\ln(1/\gamma)}\left[2\ln(1/\gamma) - 1 + \gamma^2\right] - (1-\gamma^2)^2\right\}. \tag{54}$$

Due to the no-slip boundary condition, the volumetric flow rate also reaches a plateau. As $B$ goes to zero the velocity derivative at the outer wall tends to become zero (zero shear stress) but the velocity cannot become uniform. The velocity contours for the axisymmetric annular flow and the flow in a duct of an annular-sector cross-section are compared in Fig. 13 for various values of the slip number. The velocity contours in annular Poiseuille flow are denser near the two cylinders in the case of no-slip ($B = \infty$) and the maximum velocity occurs in an intermediate radial distance. The velocity maximum moves towards and eventually reaches the outer cylinder as slip is enhanced. A similar trend is observed in the case of the annular sector (Fig. 13b) but only far from the two planar walls of the duct where the no-slip condition applies thus "pushing" the velocity contours towards the outer cylinder where slip occurs. It is clear that the greater the distance from the planar walls the stronger is the slip observed along the outer cylindrical wall.

Similar observations can be made for other values of the opening angle parameter $\alpha$ and the radii ratio $\gamma$. In Figs. 14–16 we plotted the velocity contours for $\gamma = 0$ (circular sector) and $\alpha = 0.5$, 1, and 1.5, respectively. The maximum velocity occurs at the plane $\theta = a\pi/2$ and moves towards the cylindrical wall as

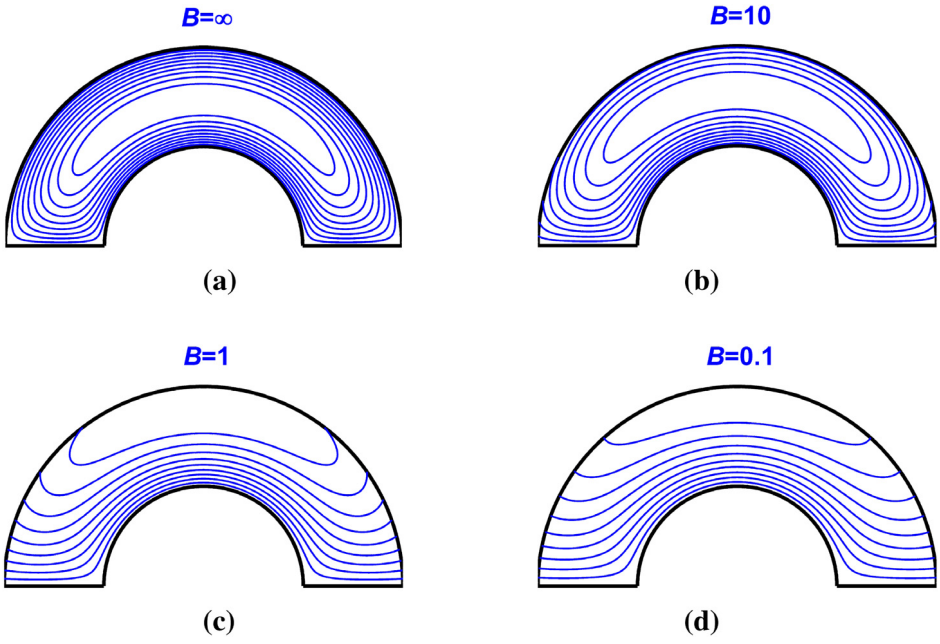


**Fig. 18.** Velocity contours for $\alpha = 1$, $\gamma = 0.5$ and various values of the slip number $B$: (a) $B = \infty$ (no slip); (b) $B = 10$ (weak slip); (c) $B = 1$ (moderate slip); (d) $B = 0.1$ (strong slip).

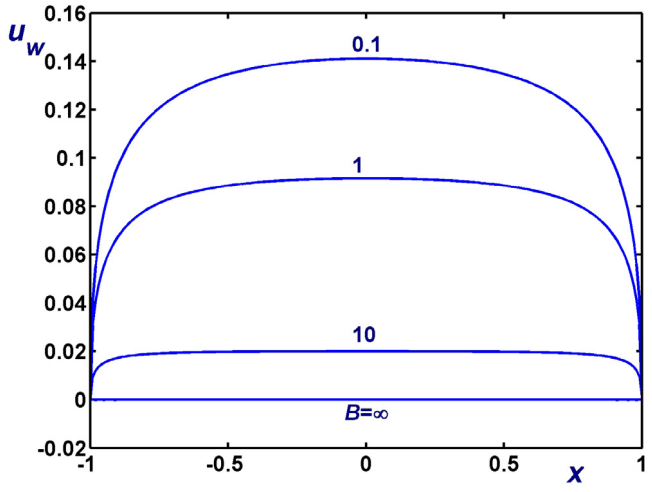


**Fig. 19.** Slip velocity for $\alpha = 1$, $\gamma = 1/2$ and various values of the slip number $B$.

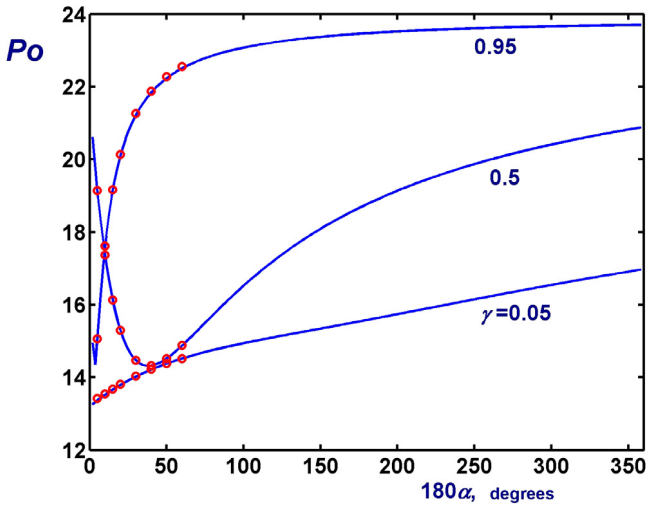


**Fig. 20.** Poiseuille numbers versus the opening angle of the angular sector for three values of the radii ratio $\gamma$ in the absence of slip. The red circles correspond to values provided by Sparrow et al. [4].

slip becomes stronger. Fig. 17 shows the slip velocities for various values of B and $\alpha = 1$, i.e. for a semicircular cross-section; the velocity contours corresponding to Fig. 17 are those of Fig. 15. The results for annular-sector cross-sections are quite similar. As an example, we show in Fig. 18 the velocity contours for $\gamma = 0.5, \alpha = 1$ and various values of the slip number. The corresponding slip velocities are shown in Fig. 19. When comparing the present results with those of Wang [5] for the flow where Navier slip applies along all the walls, we note that in the latter case the velocity tends to become more uniform as slip becomes stronger. This is not the case when slip applies only along some walls; the velocity tends to become plug only near boundaries where slip occurs.

An important quantity in the study of internal fully-developed flow is the Poiseuille number, $Po$, which represents the ratio between pressure and viscous forces. This is defined as the product of the Fanning friction factor

$$f \equiv \frac{D_h^*}{2\rho^* u_m^{*2}} \left(-\frac{dp^*}{dz^*}\right) \tag{55}$$

and the Reynolds number

$$Re \equiv \frac{\rho^* u_m^* D_h^*}{\eta^*} \tag{56}$$

where $\rho^*$ is the fluid density and $D_h^*$ is the hydraulic (or equivalent) diameter of the duct [4,17]. The latter is defined by

$$D_h^* \equiv \frac{4A^*}{P^*} \tag{57}$$

where $A^*$ and $P^*$ are the dimensionless cross-sectional area and the wetted perimeter, respectively [18]. In terms of the dimensionless variables used in the present work, the Poiseuille number is given by Wang [5]

$$Po \equiv \frac{8A^3}{P^2 Q} \tag{58}$$

where

$$A = \frac{\alpha\pi}{2}(1-\gamma^2) \quad \text{and} \quad P = 2(1-\gamma) + \alpha\pi(1+\gamma) \tag{59}$$

and therefore

$$Po \equiv \frac{\alpha^3\pi^3(1-\gamma^2)^3}{[2(1-\gamma)+\alpha\pi(1+\gamma)]^2 Q}. \tag{60}$$

In Fig. 20, we plotted the Poiseuille numbers of the no-slip case versus the opening angle of the annular sector for $\gamma = 0.05, 0.5$

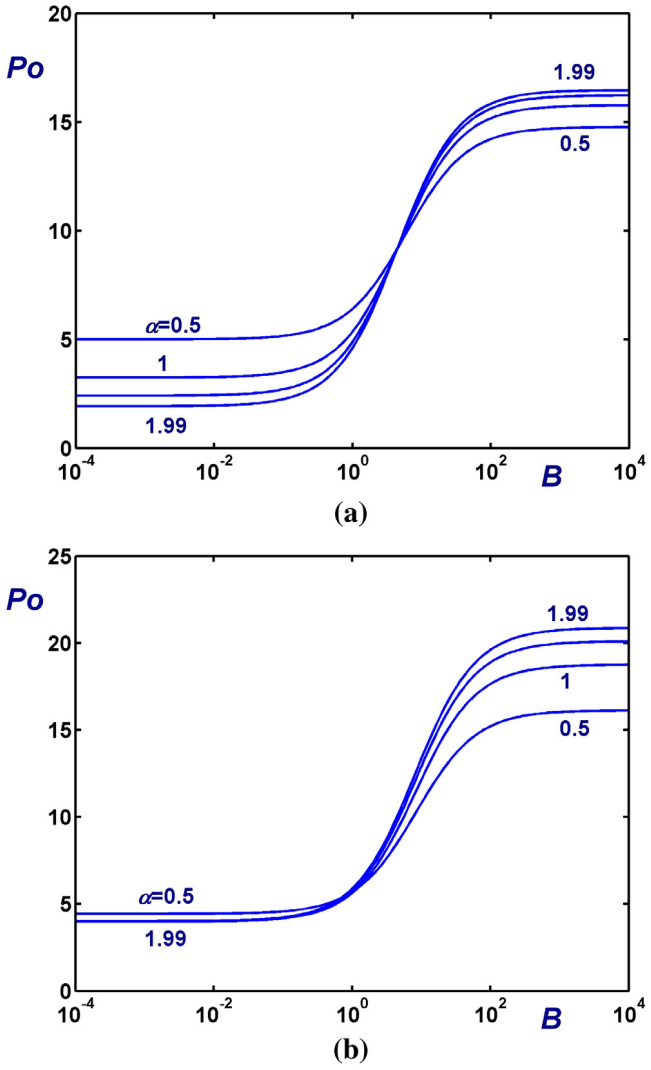


**Fig. 21.** Poiseuille numbers versus the slip number for various values of the opening angle parameter, i.e. $\alpha = 0.5$, 1, 1.5, and 1.99: (a) $\gamma = 0$ (circular sector); (b) $\gamma = 0.5$ (angular sector); the curve for $\alpha = 1.5$ lies between the curves for $\alpha = 1$ and 1.99.

and 0.95. The red circles correspond to results tabulated by Sparrow et al. [4]; to avoid crowdedness, we have not considered all the values of $\gamma$ used by the latter authors. The agreement is very good; however, it should be noted that there are some minor differences which are presumably due partly to the limited available computational tools in the early sixties and partly to the more complex expression obtained by Sparrow et al. [4] for the volumetric flow rate.

In Fig. 21 we plotted the calculated Poiseuille numbers for $\gamma = 0$ (circular sector, Fig. 20a) and 0.5 (angular sector, Fig. 20b) versus the slip number for various values of the opening angle parameter $\alpha$ (0.5, 1, 1.5 and 1.99). We observe that slip dramatically reduces the Poiseuille number, an observation also made by Wang [5] for the case where slip occurs along all the walls. The calculated values agree with values provided in the literature. For example, in the case where $\alpha = \gamma = 0.5$ and $B \to \infty$ (no slip), the Poiseuille number is Po = 16.129 which agrees well with the values of Shah and London [19] and Wang [20]. As already mentioned, when the cross-section is semicircular ($\alpha = 1, \gamma = 0$) the volumetric flow rate in the absence of slip is $Q = \pi/8 - 1/\pi$; in this case, Eq. (60) yields

$$Po \equiv \frac{8\pi^4}{(\pi+2)^2(\pi^2-8)}; \ 15.7668 \tag{61}$$

a result also reported by Wang et al. [2].

## 5. Conclusions

We have derived the analytical solution of Newtonian Poiseuille flow in ducts whose cross-sections are annular or circular sectors, allowing Navier slip to occur along the outer cylindrical wall. Some special cases as well as the more general case where slip occurs along both the cylindrical walls have also been examined. The effects of the opening angle, the radii ratio and the slip number on the velocity contours, the volumetric flow rate, and the Poiseuille number have been discussed. The present solutions compare favourably with available results in the literature. These can be useful in studies of flows in microfluidic devices [21,22] but also in applications of polymer extrusion through annular dies [13].

## Conflict of interest

The authors declare that they have no conflict of interest.

## References

[1] H.A. Stone, A.D. Stroock, A. Ajdari, Engineering flows in small devices: Microfluidics toward a lab-on-a-chip, Annu. Rev. Fluid Mech. 36 (2004) 381–411.
[2] C.Y. Wang, Y.H. Liu, C.C. Chang, Analytical solution of electro-osmotic flow in a semicircular microchannel, Phys. Fluids 20 (2008) 063105.
[3] G.I. Morini, Single-phase convective heat transfer in microchannels: a review of experimental results, Int. J. Thermal Sci. 43 (7) (2004) 631–651.
[4] E.M. Sparrow, T.S. Chen, V.K. Johnson, Laminar flow and pressure drop in internally finned annular ducts, Int. J. Heat Mass Transfer 7 (1964) 583–585.
[5] C.Y. Wang, Slip flow in an annular sector duct using radial eigenfunctions, Theoret. Appl. Mech. Lett. 4 (2014) 032002.
[6] E. Lauga, M.P. Brenner, H.A. Stone, Microfluidics: The no-slip boundary condition, in: C. Tropea, A.L. Yarin, J.F. Foss (Eds.), Handbook of Experimental Fluid Dynamics, Springer, Heidelberg, 2007, pp. 1219–1240.
[7] C. Neto, D.R. Evans, E. Bonaccurso, H.J. Butt, V.S.J. Craig, Boundary slip in Newtonian liquids: a review of experimental studies, Rep. Progr. Phys. 68 (2005) 2859–2897.
[8] F. Shapirov, V. Seleznev, Data on internal rarefied gas flows, J. Phys. Chem. Ref. Data 27 (1998) 657–706.
[9] C.L.M.H. Navier, Sur les lois du mouvement des fluides, Mé. L'Acad. Sci. L'Inst. France 6 (1827) 389–440.
[10] M.M. Denn, Extrusion instabilities and wall slip, Annu. Rev. Fluid Mech. 33 (2001) 265–287.
[11] S.G. Hatzikiriakos, Wall slip of molten polymers, Prog. Polym. Sci. 37 (2012) 624–643.
[12] S.J. Bolaños, B. Vernescu, Derivation of the Navier slip and slip length for viscous flows over a rough boundary, Phys. Fluids 29 (2017) 057103.
[13] C.Y. Wang, Slip flow in ducts, Can. J. Chem. Eng. 81 (2003) 1058–1061.
[14] G.C. Georgiou, G. Kaoullas, Newtonian flow in a triangular duct with slip at the wall, Meccanica 48 (2013) 2577–2583.
[15] Y. Damianou, G.C. Georgiou, Viscoplastic Poiseuille flow in a rectangular duct with wall slip, J. Non-Newton. Fluid Mech. 214 (2014) 88–105.
[16] J.D. Logan, Applied Mathematics, third ed., John Wiley & Sons, Inc., Hoboken, New Jersey, 2006.
[17] R. Alassar, Hagen–Poiseuille flow in tubes of semi-circular cross-sections, Proceedings of the 4th International Conference on Modeling, Simulation and Applied Optimization (ICMSAO), Kuala Lumpur, Malaysia, 19-21 April, 2011.
[18] S.W. Churchill, Viscous Flows–the Practical Use of Theory, Butterworths, Boston, MA, 1988.
[19] R.K. Shah, A.L. London, Laminar Flow Forced Convection in Ducts, Academic Press, New York, 1978.
[20] C.Y. Wang, Analytical solution for forced convection in a semi-circular channel filled with a porous medium, Transp. Porous Media 73 (2008) 369–378.
[21] J. Jang, Y.H. Kim, Gaseous slip flow of a rectangular microchannel with non-uniform slip boundary conditions, Microfluid. Nanofluid. 9 (2010) 513–522.
[22] E.M. Languri, K. Hooman, Slip flow forced convection in a microchannel with semi-circular cross-section, Int. Commun. Heat Mass Transfer 38 (2011) 139–143.